national accelerator laboratory

NAL-Pub-73/87-THY
December 1973

A Field-Theoretic Study of the Regge-Eikonal Model I

JOCHEN BARTELS*
National Accelerator Laboratory, Batavia, Illinois 60510

ABSTRACT

The Regge-eikonal model in ϕ^3 field theory is studied within the framework of Gribov's reggeon calculus. A condition is derived what sort of multi-reggeon exchange diagrams are important for large energies, and it is shown that the eikonal form is valid only in the weak-coupling limit, i.e., when the inner coupling constant of the reggeons goes to zero: $g^2 \sim 1/\ell n\, s$. The breakdown of the eikonal approximation outside of this limit is shown to be an effect of inelastic intermediate states.

---

*Most of this work has been done at II. Institut für Theoretische Physik, Universitat Hamburg, Hamburg, Germany.

I. INTRODUCTION

In recent years there have been several attempts, within simple field-theoretic models, to justify the eikonal form for the elastic scattering amplitude. The most simple class of Feynmann diagrams, having an eikonal high energy limit, are the generalized ladders, i.e., simple ladders in the s-channel with the rungs crossed in all possible ways. It has been shown in QED and ϕ^3 [1] that if one takes certain parts of these diagrams and then sums over all these ladders, one obtains the eikonal form in the high-energy limit:

$$T(s,t) \sim is \int d^2 b_\perp e^{ik_\perp b_\perp} [e^{i\chi(s,b_\perp)} - 1] \quad (-k_\perp^2 = t) \qquad (1.1)$$

$$\chi(s,b_\perp) = \frac{\text{const}}{s} \int d^2 q_\perp e^{-iq_\perp b_\perp} \frac{1}{q_\perp^2 + \mu^2} \qquad (1.2)$$

The parts of the diagrams which have been taken into account are associated with a definite path of the large momenta through the diagram, namely the eikonal path along the straight lines of the ladders. In QED the eikonal contributions are the dominant ones for large energies but not for ϕ^3.

However, since the eikonal scattering amplitude is often used as a model for Regge-cuts, phenomenologists are more interested in a theoretical study of the formula (1.1) with

$$\chi(s,b_\perp) = \frac{\text{const}}{s} \int d^2 q_\perp e^{-iq_\perp b_\perp} R(s_1 - q_\perp^2) \qquad (1.3)$$

instead of (1.2), where R(s,t) is the amplitude for the one-Regge exchange, the external masses being on the mass shell. Such an amplitude is supposed to arise from those Feynman diagrams where reggeons are exchanged between the scattering particles and the reggeon legs coupled to them in all possible orderings. (Fig. 1.) This is why people have been interested in the high-energy behavior of the s-channel iteration of ladders in ϕ^3 [2-7] and towers in QED.[8,9]

However, existing derivations[2-5,8,9] of the eikonal form of these diagrams are not satisfactory in two respects. Firstly, among the considered diagrams there are the Mandelstam diagram (Fig. 2a) and that of Amati, Fubini and Stanghellini (AFS) (Fig. 2b) and it is known[10,11] that the first has Regge-cut behavior while the second is proportional to $\ell n\, s/s$. Thus they cannot contribute equally in the high-energy limit, and any exact study must take care of this. In the earlier studies, however, all permutations in Fig. 1 seem to have the same s-behavior. Secondly, by conventional methods such as used in these papers, for each order of the coupling constant only the first leading $\ell n\, s$ -terms is found, and then their sum must not necessarily be the true high-energy behavior of the infinite sum of Feynman diagrams. In fact, this leading term summation leads to the combined limit $s \to \infty$, $g^2 \sim 1/\ell n\, s$ (weak coupling limit):

$$s \to \infty, \quad g^2 \ell n\, s = \text{const} \tag{1.4}$$

In the present paper an attempt is made to perform a study of the Regge-eikonal model without these two defects. Since we want to find the high-energy behavior at fixed coupling constants, we cannot proceed in the conventional way of summing leading ℓn s-terms. Instead of this, we use for the exchanged reggeons Bethe-Salpeter amplitudes and place them into the Feynman diagrams (Fig. 1). We are, of course, not able to find the exact solutions of the Bethe-Salpeter equation, but for our purposes it is sufficient to know its analytic properties and, for control, the limit $g^2 \to 0$. To find the high-energy behavior of the amplitudes of multiregge exchange we use the reggeon-calculus of Gribov.[12] The result obtained in this way is expected to be valid for all values of the coupling constant.

This is the technique we shall use for our study of the diagrams in Fig. 1, first in ϕ^3 and afterwards in QED. Our main task will be a detailed study of the Gribov vertices, which couple the reggeons to the scattering particles and are in general multidimensional integrals over the internal momenta. For eikonalization, they must decouple into a produce of reggeon vertex functions, as it can be seen by expanding the exponential in (1.1). Such a decoupling holds only when the internal coupling constant of the reggeons goes to zero as in (1.4). Otherwise, the eikonal form does not emerge. We show that the breaking parts, which can be neglected only in the weak coupling limit, belong to inelastic intermediate states between the successive exchange of

reggeons. Thus our study within a simple field theoretic model of the eikonal approximation confirms that (1.1) is not valid because of the neglect of inelastic contributions. In the framework of ϕ^3 the breakdown of the eikonal approximation has already been shown,[6,7] but no interpretation of the breaking terms has been given. Besides this interpretation we find that only a certain subgroup of the diagrams of Fig. 1 contributes to the leading high energy behavior. This is analogous to the situation of the Mandelstam diagram and that of AFS: The Gribov vertex, considered as a particle-particle multireggeon amplitude, must have a certain singularity structure in its subenergies.

In this first paper we treat the ϕ^3 case. In Sec. II we describe our calculation scheme, which is based on the pertubation theoretical derivation of Gribov s reggeon calculus. Application of this technique to the diagrams of Fig. 1 shows that (1.1) is not correct. Furthermore, we consider the Gribov vertices as reggeon-particle amplitutudes and find, as a consquence of its analytical properties, that certain structures of Fig. 1 are unimportant. In the next section we let g^2 approach zero as in (1.4) and see how eikonalization appears. A physical interpretation is given in Sec. IV. In a following paper our considerations will be extended to QED.

II. MULTIREGGE EXCHANGE

The derivation[12] of Gribov's reggeon calculus, as a prescription

for the calculation of the high-energy behavior of certain Feynman diagrams, is based on the assumption that, e.g., for the two-reggeon exchange in Fig. 3a, the high-energy behavior is determined by those parts of the momentum integrations in the upper and lower parts, where the legs of the reggeons are not infinitely far from their mass-shell and the momentum transfer through the reggeons is finite, too. When the reggeons are built up by ϕ^3-ladders, this assumption is justified because of damping properties of the reggeon amplitude for large values of its external masses and momentum transfer. As a result of this, the region of momentum integration can be restricted and the expressions for the Feynman propagators simplify. The most convenient way to see this is the introduction of Sudakov variables or, equivalently, infinite momentum variables ($p_+ = p_0 + p_3$, $p_- = p_0 - p_3$, $p_\perp$). For our considerations we choose the latter ones.

For an illustration of these approximations in terms of infinite momentum variables we write down the expression for Fig. 3a. The reggeons are assumed to be ladders and have the factorized form:

$$R(p_1^2, p_1'^2; p_2^2, p_2'^2; s,t) = b(p_1^2, p_1'^2; t) s^{\alpha(t)} \xi(t)\ b(p_2^2, p_2'^2; t) \qquad (2.1)$$

$$\xi(t) = 1 + e^{-i\pi\alpha(t)}$$

and we use a reference system where the upper particle has only a (large) 3-component along the positive direction, the lower along the negative direction. Starting with the upper part of the diagram, we introduce

the notations:

$$(r_2)_z = -(r_3)_z \sim \omega + \frac{1}{2\omega}(r_{1\perp}^2 + M^2)$$

$$(r_2)_+ = (r_3)_- = 2\omega$$

$$(r_2)_- = (r_3)_+ = \frac{M^2}{2\omega} \qquad (2.2)$$

$$(r_1)_0 = (r_1)_z = 0$$

$$(p_i)_+ = 2\omega x_i; \qquad 2\omega(p_i)_- = y_i$$

$$2\omega(q)_- = y$$

In the propagators we everywhere neglect the q_+ component with respect to the p_{i+} and all terms $\sim \frac{1}{\omega}$:

$$(r_2 - p_1)^2 \sim (1 - x_1)(r_{1\perp}^2 + M^2 - y_1) - p_{1\perp}^2$$

$$(r_2 - p_1 - p_2 - q)^2 \sim (1 - x_1 - x_2)(r_{1\perp}^2 + M^2 - y_1 - y_2 - y) - (p_1 + p_2 + q)_\perp^2$$

$$(r_2 + r_1 - p_1 - q)^2 \sim (1 - x_1)(r_{1\perp}^2 + M^2 - y_1 - y) - (r_1 - p_1 - q)_\perp^2$$

$$(p_2 - r_1)^2 \sim x_1 y_1 - (p_1 - r_1)_\perp^2$$

$$(p_1 + q)^2 \sim x_1(y_1 + y) - (p_1 + q)_\perp^2 \qquad (2.3)$$

$$(p_2 + q)^2 \sim x_2(y_2 + y) - (p_2 + q)_\perp^2$$

$$(p_2 + r_1)^2 \sim x_2 y_2 - (p_2 + r_1)_\perp^2$$

$$(p_1 + p_1')^2 \sim (p_{1+} p_{1-}') = (2\omega)^2 x_1 x_1' = s\, x_1 x_1'$$

we have to take care of double counting by a factorial $1/n!$. Thus the general form of the amplitude with the exchange of n reggeons is:

$$T_n(s,t) = 2is\,\frac{(2\pi)^2}{n!}\left[\frac{-i}{2(2\pi)^2 s}\right]^n \int d^2q_{1\perp}\ldots d^2q_{n\perp}\,\delta^{(2)}(\Sigma q_{i\perp} - 2r_{1\perp})$$

$$\times\,[I_n(r_1, q_1 \ldots q_{n\perp})]^2 P_1(s,q_1)\ldots P_n(s,q_n)$$

$$P_i(s,q_i) = S^{\alpha(-q_{i\perp}^2)}\,\xi(-q_{i\perp}^2) \qquad (2.6)$$

where the Gribov vertex I_n is the sum of all structures in Fig. 1.

Expanding the exponential of the eikonal formula (1.1) and comparing the n^{th} order term with (2.6) we see that in order to reproduce the eikonal form the Gribov vertex functions must factorize into a product of n reggeon vertex functions, their external masses being on the mass shell. Thus we have to see whether and under what conditions such a factorization is valid. It will be necessary to perform the y-integrations in (2.5), and this can be done most easily if we use a spectral representation for the reggeon vertex function, which contains the analytical structure in the external masses and in momentum transfer:

$$b(p_1^2, p_1'^2; t) = \int_{-1}^{+1} dx \int_{\zeta_0}^{\infty} d\zeta\, \frac{\bar{\rho}(\zeta, z)}{\zeta - \frac{1+z}{2}p_1^2 - \frac{1-z}{2}p_1'^2 + \frac{1-z^2}{4}t - i\epsilon} \qquad (2.7)$$

$$b(p_1^2, p_1^2; t) \quad \frac{1}{p_1^2 - m^2} \quad \frac{1}{p_1'^2 - m^2}$$

The primed momenta belong to the lower part, which is treated in a similar way. Since q_+ does not occur in the upper part, and q_- in the lower, the amplitude factorizes with respect to these two integrations:

$$T(s,t) = 2is\,(2\pi)^2\left(\frac{-i}{8\pi^2 s}\right)^2\int d^2q\,\left[I_{3a}(r_{1\perp}, q_\perp)\right]^2 S^{\alpha[-(r_1+q)_\perp^2]}\xi[-(r_1+q)_\perp^2]$$
$$\times S^{\alpha[-(r_1-q)_\perp^2]}\xi[-(r_1-q)_\perp^2] \qquad (2.4)$$

$$I_{3a}(r_{1\perp}, q_\perp) = \left[\frac{ig^2}{2(2\pi)^4}\right]^2\int\frac{dy}{2\pi i}\int dx_1 dx_2 dy_1 dy_2 d^2p_{1\perp} d^2p_{2\perp}\, x_1^{\alpha[-(r_1+q)_\perp^2]}\, x_2^{\alpha[-(r_1-q)}$$

$$\times\frac{1}{(r_2-p_1)^2-m^2}\;\frac{1}{(r_2-p_1-p_2-q)^2-m^2}\;\frac{1}{(r_2+r_1-p_1-q)^2-m^2}$$

$$\times b\left[(p_1-r_1)^2,(p_1+q)^2;(r_1+q)^2\right]\frac{1}{(p_1-r_1)^2-m^2}\;\frac{1}{(p_1+q)^2-m^2}$$

$$\times b\left[(p_2+q)^2,(p_2+r_1)^2;(r_1-q)^2\right]\frac{1}{(p_2+q)^2-m^2}\;\frac{1}{(p_2+r_1)^2-m^2} \qquad (2.5)$$

where in (2.5) the approximations (2.3) have to be inserted. From the y-integrations we obtain the condition that there must be always singularities in both the upper and lower half plane, and this restricts the x integrations to the interval (0,1).

The form (2.4) holds for all structures of Fig. 1. When we sum over all permutations of the reggeon legs at the upper and lower line,

$$= \int_{-1}^{+1} dz \int_{\zeta_0}^{\infty} d\zeta \frac{\rho(\zeta_1 z)}{(\zeta - \frac{1+z}{2} p_1^2 - \frac{1-z}{2} p_1'^2 + \frac{1-z^2}{4} t - i\epsilon)^3}$$

$$= \int dZ \frac{\rho(Z)}{(\zeta - \frac{1+z}{2} p_1^2 - \frac{1-z}{2} p_1'^2 + \frac{1-z^2}{4} t - i\epsilon} \qquad (2.8)$$

This spectral form is justified[13,14] at least for our ϕ^3-ladders, but they are assumed to be still of more general validity.

With this ansatz we return to (2.5) and the corresponding expression for Fig. 3b-d, perform the y-integrations. There is no evidence for a factorization of the Gribov vertex. Thus we conclude that the eikonal form (1.1) cannot be justified within our model. In the next section we shall see that the situation changes when we take the weak coupling limit.

For the rest of this section we concentrate on the question what sort of structures and permutations at the upper and lower line if Fig. 1 are important in the high-energy limit. For this we perform the y-integrations, within (2.5) and similar expressions for other diagrams of Fig. 1, and find the following: only those structures give a result different from zero, where--following within the upper or lower part the straight line from the incoming particle to the outgoing one--first all reggeons have to be emitted in an arbitrary order, before any reggeon is absorbed again. We call them "nested" diagrams, and one counter-example is given in Fig. 4.

The remaining structures are zero in our formalism, since for some of the y-integrations all singularities are located in one half-plane and the integration contour can be closed in the other half-plane without singularities. This means that the high-energy behavior of these diagrams is much weaker than that of the nested ones.

This is quite analogous to the situation of the Mandelstam and AFS diagrams (Fig. 2). The latter has no Regge-cut behavior[10,11] and behaves as $\ell n\, s/s$ for large energies. In the Gribov calculus the vertices of this diagram turn out to be zero, since for the y-integration all singularities are in the lower half plane and the contour can be closed in the upper one. Thus the vanishing is due to singularity structure of the Gribov vertex in the y-variable. When the Gribov vertex is considered as a reggeon-particle → reggeon-particle amplitude (Fig. 5), the y-variable is just the energy, and for the AFS-structure, there are only right-hand singularities, but no left-hand ones (the third spectral function is zero). Therefore, a necessary condition for the nonvanishing of a Regge-cut amplitude is the existence of both right and left-hand singularities in the energy-variable of the reggeon-particle scattering amplitudes.

For the exchange of n reggeons one has to generalize this argument. At the upper and lower end of the amplitude there are now pieces (Fig. 6) which represent amplitudes with two particles and n reggeons, integrated over n-1 independent subenergies (e.g., the s_k in Fig. 6; s_k is the subenergy of the left particle together with the first k reggeons). For

our diagrams of Fig. 1 with the notation of Fig. 7, the subenergies s_k are given by the $(q_{ij})_-$:

$$s_k = (r_2 - r_1 + q_{12} - q_{10} + \ldots + q_{KK+1} - q_{KK-1})^2$$

$$= (r_2 + q_{KK+1})^2$$

$$\sim 2\,\omega q_{KK+1}$$

$$= y_{KK+1} \qquad (2.9)$$

and the Gribov vertices can be written as:

$$I = \int_{-\infty}^{\infty} ds_1 \ldots ds_{n-1}\, A(s_1, \ldots s_{n-1}; \ldots) \qquad (2.10)$$

A is the two-particle n-reggeon amplitude and depends still on onther variables than the s_k (e.g., the reggeon masses). Equation 2.10 will be different from zero only when A has right and left-hand singularities in all subenergies s_k. Otherwise one could close the contour in one half-plane that is free from singularities and obtains zero. In Fig. 4 this can be illustrated, when we use the energies s_1 and s_2 as indicated. Then there is at fixed s_2 for s_1 only a right-hand cut. As similar situation holds for all non-nested diagrams, as it can be seen by appropriate choices of subenergies.

For the nested graphs we still rewrite (2.10) by turning around the integrations paths:

$$I = \int_{s_{10}}^{\infty} ds_1 \cdots \int_{s_{n-10}}^{\infty} ds_{n-1}\, \mathrm{disc}_{s_1 \cdots s_{n-1}} A \qquad (2.11)$$

where s_{k0} are the thresholds in the s_k-channels and the discontinuity has to be taken across the cuts in all subenergies.

That only the nested graphs are important for large energies is not obvious from other studies of the multi-ladder exchange in ϕ^3. There all structures of Fig. 1 are of the same order in s and no distinction is made between the AFS and Mandelstam diagram.

III. THE WEAK-COUPLING LIMIT

All results of the last section are valid for the limit $s \to \infty$ and fixed coupling constant. We now shall see how in the weak-coupling limit (1.4) the situation changes and the Gribov vertices I_n of (2.6) split up into a product of the reggeon vertex function, just as it was found to be necessary for the eikonal form. The limit (1.4) is reached, when we calculate the limit $g^2 \to 0$ of the Gribov vertex (2.8) and similar expressions for the other structures. For this we need some properties of the spectral form (2.4) and the trajectory function $\alpha(t)$ in this limit. They are derived in the appendix by means of the Bethe-Salpeter equations:

$$\alpha(t) \underset{g^2 \to 0}{\sim} -1 + \frac{g^2}{16\pi^2} \int_0^1 dx \, \frac{1}{-x(1-x)t + m^2 - i\epsilon} \qquad (3.1)$$

$$= -1 + \frac{g^2}{16\pi^2}\,\alpha_0(t)$$

$$\rho(\zeta, z) \xrightarrow[g^2 \to 0]{} ig \tag{3.2}$$

$$\rho(\zeta, z) \xrightarrow[\zeta \to \infty]{} \zeta^{-\alpha - 1}\,\rho_\infty(z), \quad \rho_\infty(z) \xrightarrow[g \to 0]{} ig \tag{3.3}$$

One easily checks that this behavior is in accordance with the well-known weak-coupling result[15]:

$$b(p_1^2, p_1'^2; t) \xrightarrow[g^2 \to 0]{} ig \tag{3.4}$$

Now we return to (2.5). In the limit $g^2 \to 0$ the trajectory function approaches -1 and the x-integrations in (2.5) diverge at the point $x_i = 0$. To see this in more detail we use the spectral form (2.8) and perform the y-integrations by picking up the poles in one half plane;

$$\left(\frac{g^2}{2(2\pi)^3}\right)\int d^2p_{1\perp}\, d^2p_{2\perp} \int_0^1 dx_1 \int_0^{1-x_1} dx_2\, \frac{x_1^{\alpha[-(r_1+q)_\perp^2]}\, x_2^{\alpha[-(r_1-q)_\perp^2]}}{(1-x_1)^2\,(1-x_1-x_2)}$$

$$\times \int dZ_1 dZ_2 \rho(Z_1)\rho(Z_2)\, \frac{1}{2^2}\, \frac{\partial^2}{\partial \zeta_1^2}\, \frac{\partial^2}{\partial \zeta_2^2} \left[\frac{1}{D_1^a}\, \frac{1}{\frac{x_2}{x_1}\,\mathrm{Max}\left(\frac{1+z_2}{1+z_1}, \frac{1-z_2}{1-z_1}\right) D_1^a + D_2^a}\right]$$

$$D_1^a = D_1 - x_1\,\frac{1+z_1}{2}\left[M^2 - \frac{(r_2-p_1)_\perp^2 + m^2}{1-x_1}\right] - x_2\,\frac{1-z_1}{2}\left[M^2 - \frac{(r_1-p_1-q)_\perp^2 + m^2}{1-x_1}\right.$$

$$D_2^a = D_2 - x_1 \frac{1+z_2}{2}\left[\frac{(r_2-p_1)_\perp^2+m^2}{1-x_1} - \frac{(p_1+p_2+q)_\perp^2+m^2}{1-x_1-x_2}\right]$$

$$- x_2 \frac{1-z_2}{2}\left[\frac{(r_1-p_1-q_1)_\perp^2+m^2}{1-x_1} - \frac{(p_1+p_2+q)_\perp^2+m^2}{1-x_1-x_2}\right] \qquad (3.5)$$

$$D_1 = \zeta_1 + \frac{1+z_1}{2}(p_1-r_1)_\perp^2 + \frac{1-z_1}{2}(p_1+q)_\perp^2 - \frac{1-z_1^2}{4}(r_1+q)_\perp^2$$

$$D_2 = \zeta_2 + \frac{1+z_2}{2}(p_2+q)_\perp^2 + \frac{1-z_2}{2}(p_1+q)_\perp^2 - \frac{1-z_2^2}{4}(r_1-q)_\perp^2$$

Apart from $x_i = 0$ there are also divergencies at $x_i = 1$. First we take the point $x_1 = x_2 = 0$. In the limit $g^2 \to 0$, the integral (without the constant factor in front of it) is found to diverge proportional to $1/g^4$, and the coefficient is found by partial integration with respect to the x_i:

$$(ig)^2 \frac{\alpha_0[-(r_1+q)_\perp^2]}{\alpha_0[-(r_1+q)_\perp^2] + \alpha_0[-(r_1-q)_\perp^2]} \qquad (3.6)$$

Similarly, the expression for Fig. 3b contains a divergence at $x_1 = x_2 = 0$, too, and its contribution is (3.6) with $q_\perp$ replaced by $-q_\perp$, because Fig. 3a and b differ only by the interchange of the reggeons. The sum of these two contributions is $(ig)^2$, the square of the reggeon vertex function in the weak-coupling limit (3.4). The corresponding two-reggeon exchange amplitude has the eikonal form:

$$T_2(s,t) = 2is\,\frac{(2\pi)^2}{2!}\left(\frac{-i}{8\pi^2 s}\right)^2 \int d^2q_\perp\,(ig)^4\, s^{\alpha[-(r_1-q)_\perp^2]}\,\xi[-(r_1-q)_\perp^2]$$

$$\times\, s^{\alpha[-(r_1+q)_\perp^2]}\,\xi[-(r_1+q)_\perp^2] \qquad (3.10)$$

When $x_1 = x_2 = 0$, the large momenta of the incoming particles are restricted onto the straight lines through the diagram, and since these lines are responsible for the eikonal form, they will be called the "eikonal path".

We are still left with the other divergent point of (3.5) at $x_1 = 1$ and $x_2 = 0$. This point is associated with another path of the large momenta through the diagram, and its divergence is also proportional to $1/g^4$. However, we shall not take into account this contribution and confine ourselves to the eikonal paths. The reason for this will be discussed at the end of this section. For the remaining structures of Fig. 3c,d, one can show that in the limit $g^2 \to 0$ there are only divergencies $1/g^2$, and thus they are less important in the weak-coupling limit.

A similar study of the n-reggeon case shows the following generalization: in the limit $g^2 \to 0$, only a certain subgroup of the nested diagrams, those of Fig. 8, are important, and their eikonal path contributions add up to a factorizing Gribov vertex $(ig)^n$. The diagrams of Fig. 8 will be called the "maximal nested" ones (in accordance with Ref. 4), since on the straight line all reggeons are completely contained in other reggeons. For the remaining,

non-maximal nested diagrams, it can be shown that they have weaker divergencies in the x-integrations and thus go stronger to zero when $g^2 \to 0$ than the maximal nested diagrams.

We still have to explain our neglect of the noneikonal paths. As we have seen, in the weak-coupling limit the Gribov vertices are determined by definite points in the x-integrations, and these points can be associated with definite paths of the large momenta through the diagram. They are the same as the t-paths of Tictopoulos,[16] and the leading behavior of a diagram always belongs to the shortest t-path. For diagrams like that of Fig. 8 the shortest path runs along the legs of the lowest reggeon and is more important than the eikonal path along the straight line. Thus the eikonal form cannot be the true high-energy behavior. But this is a specific feature of ϕ^3 theory. In QED, as we shall show in a following paper, the spin numerators along the straight electron lines suppress all other paths than the eikonal one. Apart from this dominance of paths, the situation is the same as in ϕ^3, and thus the eikonal form in QED represents the true high-energy behavior. The ϕ^3 study in the present paper is to be considered as a preparation of the more realistic QED-model, and this is why we neglect here complications, that arise only in ϕ^3 and not in QED.

Before we come to a more physical interpretation of what happens in the n-reggeon exchange amplitudes at $g^2 \to 0$, we want to comment the limit (1.4). A brief consideration of the high-energy behavior of a simple

t-channel ladder shows that the approximation

$$b^2(p_1^2, p_2^2; t)\, s^{\alpha(t)} \rightarrow (ig)^2\, s^{-1 + g^2/16\pi^2\, \alpha_0(t)} \tag{3.11}$$

is valid when $s \rightarrow \infty$, but $\ell n\, s\, g^2 = \text{const}$. The right-hand side of (3.11) is derived[15] by the usual summation over leading ℓn s-terms in each order of the coupling constant, and we conclude that this technique derives the weak-coupling limit (1.4) but not the more interesting limit $s \rightarrow \infty$ and g^2 fixed. On the other hand, the weak-coupling limit of our approach should lead to the same result as the leading term summation. This is indeed the case, as we can see by comparing Ref. 4 with our results. There it is assumed that the maximal nested diagrams are the leading ones in each order (by powers of ℓn s stronger than non-maximal nested), and the eikonal form is derived. Our study leads to the same result, because the statement that in the weak-coupling limit the non-maximal nested diagrams are weaker by powers of g^2 is equivalent to the statement that--for a given order of the coupling constant--diagrams with non-maximal structures are lower than the maximal nested ones by powers in ℓn s.

IV. INTERPRETATION OF THE BREAKDOWN OF THE EIKONAL APPROXIMATION

We finally come to a physical interpretation of that what happens in the weak-coupling limit. The variables x_i, as defined in (2.5), are

fractions of the large incoming momenta, and the condition of the non-vanishing of the y-integration restricts them to the interval (0, 1). Outside of the weak-coupling limit, there is no evidence of eikonalization, since the whole x-interval contributes. In the weak-coupling limit, only the end points of the interval become important, and they correspond to a definite path of the large momenta through the diagram. One of these paths runs along the straight lines of the scattering particles and its contribution yields the eikonal form. Thus it is a characteristic feature of the eikonal approximation, that the scattering particles retain their large momenta during the scattering process and interact via the emission and absorption of soft reggeons. This is completely equivalent to the eikonalization of exchange of virtual particles (generalized ladders).

This picture follows immediately from our choice of variables and approximation rules. For a better understanding, however, it is useful to consider the situation also from another side. For this we return to the form (2.11) of the Gribov vertex. The integrand of this representation is obtained from A by taking the discontinuities across the subenergy singularities (in our notation, the s_k are identical to the y_{KK+1}). If A were a usual Feynman diagram with n+2 external particles, we would obtain the discontinuities by cutting the internal lines and using the Wick-Cutcosky rules.[17] But A is an amplitude with 2 particles and n reggeons, and the latter are coupled to the internal lines of A through the reggeon vertex functions $b(m_1^2, m_2^2; t)$ instead of coupling constants for particles.

These functions b have already cuts in its mass variables, as it can be seen by replacing the reggeons by ladders. For the calculation of discontinuities of A one has to cut not only the internal lines of A, but also those of b, and then to apply the Wick-Cutkosky rules. In this way, one obtains for the Gribov vertex a decomposition into a sum of terms, each of which corresponds to a certain intermediate state (Fig. 9 for the two-reggeon case). Such a decomposition holds for all structures of A,[18,19] and the eikonal approximation is obtained from it by picking up only the elastic intermediate state. For the two-reggeon cases:

$$\mathrm{disc}_s\, A(s,t,\text{reggeon masses}) = b^2 \cdot \delta(s-m^2) + \text{inelastic contributions} \tag{4.1}$$

and from this:

$$I = \int_{m^2}^{\infty} ds\, \mathrm{disc}_s\, A = b^2 + \text{inelastic contributions} \tag{4.2}$$

(b is the coupling function of the reggeon to the particle line, the particle masses being on-mass shell). For the neglect of the inelastic contributions, however, there is no justification, and the eikonal form is not valid.

In the weak-coupling limit, only the term with the lowest power of g^2 in the decomposition (4.1) is important, and because of (3.4): $b \to ig$, this is the elastic contribution. Thus the weak-coupling limit suppresses all inelastic contributions, and yields the eikonal form. It is useful to see this in more detail, because in (4.2) there may be some

cancellations between elastic and inelastic terms. For the AFS-diagram (Fig. 2b) it is known[11] that the elastic contribution is exactly cancelled by the sum of all other terms, and this means that in the weak coupling limit, parts of the two-particle contributions must be equal to the elastic terms and proportional to g^2. In the Mandelstam diagram (Fig. 2a), there is no one-particle intermediate state at all, but such as in the AFS-diagram, the two-particle contribution in the weak-coupling limit equals the one-particle elastic term and there are no other contributions that could cancel this. Thus, in the weak-coupling limit, the Mandelstam diagram has only the elastic intermediate state and takes the eikonal form. All this can be generalized to three and more reggeons.

V. CONCLUSIONS

We have considered the breakdown of the eikonal approximation from two points of view. In the first case, we used a parton-like picture and found that eikonalization holds when the scattering particles retain their large momenta during the scattering process. Emission and absorption of reggeons can be interpreted as a fragmentation of the particles, and in the case of eikonalization their momenta are small in comparison with that of the scattering particle. This is not in agreement with the parton picture of hadrons, and the eikonal approximation must fail.

We also interpreted the situation in terms of Gribov's reggeon calculus. There the Gribov vertex can be written as an integral over

energy-discontinuities of particle-reggeon amplitudes and decomposed into contributions of different intermediate states. The eikonal form arises, when only the elastic intermediate state is taken into account, but the neglect of other contributions is not justified. Only in the weak-coupling limit the inelastic terms are suppressed, and the eikonal form is true.

From the second explanation it becomes clear which corrections should be added to the eikonal formula. They must contain the contribution of all inelastic states, but, unfortunately, we have no evidence that they have any simple form, as it is desirable for practical applications.

ACKNOWLEDGMENTS

I would like to express my gratitude to Professor G. Kramer for his very helpful discussions. For illuminating remarks during the final stage of the work I am indebted to Professor V.N. Gribov, and the Leningrad Institute of Nuclear Research for his kind hospitality.

APPENDIX

In this appendix we shall derive some properties of the spectral representation (2.7), (2.8) for ϕ^3 ladders. For this we use the same technique and approximations as in Sec. II. First we write down the Bethe-Salpeter equation for the ladders (Fig. 10), neglect the inhomogenous term and insert the spectral ansatz for the solution. The denominators are decomposed according to Ref. 13 in the following form:

$$\frac{1}{(r_2-p)^2-\mu^2}\;\frac{1}{\zeta-\frac{1+z'}{2}(p-r_1)^2-\frac{1-z'}{2}(p+r_1)^2+\frac{1-z'^2}{4}(2r_1)^2}\;\frac{1}{(p-r_1)^2-m}\;\frac{1}{(p+r_1)^2-m^2}$$

$$=\frac{1}{(r_2-p)^2-\mu^2}\;\frac{1}{\zeta'-\frac{1+z'}{2}(p-r_1)^2-\frac{1-z'}{2}(p+r_1)^2+\frac{1-z'^2}{4}(2r_1)^2}$$

$$\times\left[\frac{1}{(p-r_1)^2-m^2}\;\frac{1}{(p+r_1)^2-m^2}+\left(\frac{\frac{1+z'}{2}}{(p-r_1)^2-m^2}+\frac{\frac{1-z'}{2}}{(p+r_1)^2-m^2}\right)\right.$$

$$\left.\times\;\frac{1}{\zeta'-\frac{1+z'}{2}(p-r_1)^2-\frac{1-z'}{2}(p+r_1)^2+\frac{1-z'^2}{4}(2r_1)^2}\right] \qquad (A.1)$$

Now we use the same approximations as in Sec. II, perform the p_- and $p_\perp$ integrations by taking the residues and by symmetrical integrations, respectively, and obtain for the spectral function the integral equation:

$$\tilde{\rho}(\zeta,z)=\frac{g^2}{8(2\pi)^2}\int_{-1}^{+1}dz'\int_{\zeta_0(z)}^{\infty}d\zeta'\;K(\zeta,z;\zeta',z')\,\tilde{\rho}(\zeta',z') \qquad (A.2)$$

Here we have used the following abbreviations:

$$K(\zeta, z; \zeta', z') = \int_0^1 dx\, x^{\alpha[(2r_1)^2]-1} \frac{\delta\left[\frac{M(z)^2}{x} - \frac{\mu^2}{1-x}\right] - \delta\left[\frac{\tilde{M}(z)^2}{x} - \frac{\mu^2}{1-x}\right]}{\zeta' - M(z')^2} \tag{A.3}$$

$$M(z)^2 = \frac{1+z}{2} m^2 + \frac{1-z}{2} m^2 - \frac{1-z^2}{4} (2r_1)^2 \tag{A.4}$$

$$\tilde{M}(z)^2 = \begin{cases} \frac{1+z}{2} \dfrac{\zeta' - \frac{1-z'}{2} m^2 + \frac{1-z'^2}{4} (2r_1)^2}{\frac{1+z'}{2}} + \frac{1-z}{2} m^2 - \frac{1-z^2}{4}(2r_1)^2 & z < z' \\ \frac{1+z}{2} m^2 + \frac{1-z}{2} \dfrac{\zeta' - \frac{1+z'}{2} m^2 + \frac{1-z'^2}{4} (2r_1)^2}{\frac{1-z'}{2}} - \frac{1-z^2}{4}(2r_1)^2 & z > z' \end{cases} \tag{A.5}$$

$$\bar{\zeta}_0(z) = \left[M(z) + \mu\right]^2 \tag{A.6}$$

From this we first derive the large-ρ-behavior. After performing the x-integration by means of the δ-function we find:

$$K(\zeta, z; \zeta', z') \underset{\zeta \to \infty}{\sim} \zeta^{-\alpha(t)-1} \frac{[M(z)^2]^{\alpha(t)} - [\tilde{M}(z)^2]^{\alpha(t)}}{\zeta' - M(z)^2} \tag{A.7}$$

$$\bar{\rho}(\zeta, z) \underset{\zeta \to \infty}{\sim} \zeta^{-\alpha(t)-1} \bar{\rho}_\infty(z) \tag{A.8}$$

$$\bar{\rho}_\infty(z) = \frac{g^2}{8(2\pi)^2} \int_{-1}^{+1} dz' \int_{\bar{\zeta}_0(z')}^{\infty} d\zeta' \frac{[M(z)^2]^{\alpha(t)} - [\tilde{M}(z)^2]^{\alpha(t)}}{\zeta' - M(z')^2} \bar{\rho}(\zeta', z') \tag{A.9}$$

Now we take the limit $g^2 \to 0$. In order to have the same power of g^2 on both sides of (A.9), there must be one divergent integration in the limit $g^2 \to 0$, which cancels the factor g^2 in front of the integral. Such a divergence is achieved since

$$\alpha(t) \xrightarrow[g^2 \to 0]{} -1 + \frac{g^2}{16\pi^2}\,\alpha_0(t) \tag{A.10}$$

where $\alpha_0(t)$ has to be determined by the integral equation. For $\alpha \sim -1$ we may neglect the second term in (A.9) because of the ρ-dependence in $M(z)^2$ and obtain in the limit $\alpha \to -1$:

$$\bar{\rho}_\infty(z) = \frac{g^2}{8(2\pi)^2}\,\frac{1}{M(z)^2}\,\frac{16\pi^2}{g^2\alpha_0(t)}\int_{-1}^{+1} dz'\,\bar{\rho}_\infty(z') \tag{A.11}$$

Integrating both sides with respect to z, we have:

$$\alpha_0(t) = \int_0^1 dx\,\frac{1}{-x(1-x)t + m^2} \tag{A.12}$$

in accordance with perturbation theoretical calculations.[16] But there is still one unknown constant, an overall factor of $\bar{\rho}_\infty$, which cannot be determined from our homogeneous integral equation. This constant can be found, since we know the weak-coupling limit of the vertex function (3.11): $b(m_1^2, m_2^2; t) \to ig$. This yields:

$$ig = \lim_{g^2 \to 0} \int_{-1}^{+1} dz \int_{\bar{\zeta}_0}^{\infty} d\zeta\,\frac{\rho(\zeta, z)}{\zeta - \frac{1+z}{2}m^2 - \frac{1-z}{2}m^2 + \frac{1-z^2}{4}t}$$

$$= \frac{16\pi^2}{g^2 \alpha_0(t)} \int_{-1}^{+1} dz' \lim_{g^2 \to 0} \bar{\rho}_\infty (z') \qquad (A.13)$$

and

$$\lim_{g^2 \to 0} \bar{\rho}_\infty (z) = \frac{ig^3}{8(2\pi)^3} \frac{1}{M(z)^2} \qquad (A.14)$$

Next we are interested in the representation (2.8):

$$\frac{1}{k_1^2 - m^2} \frac{1}{k_2^2 - m^2} \int_{-1}^{+1} dz \int_{\zeta_0(z)}^{\infty} d\zeta \frac{\bar{\rho}(\zeta, z)}{\zeta - \frac{1+z}{2} k_1^2 - \frac{1-z}{2} k_2^2 + \frac{1-z^2}{4} t} \qquad (A.15)$$

We combine the denominators by means of the Feynman identity and introduce by δ-functions new variables:

$$(A.15) = \int_{-1}^{+1} dz \int_{\zeta_0(z)}^{\infty} d\zeta \frac{\rho(\zeta, z)}{\left(\zeta - \frac{1+z}{2} k_1^2 - \frac{1-z}{2} k_2^2 + \frac{1-z^2}{4} t\right)^3} \qquad (A.16)$$

$$\zeta_0(z) = M(z)^2 = m^2 - \frac{1-z^2}{4} t \qquad (A.17)$$

where the new spectral function is connected with the other one by:

$$\rho(\zeta, z) = \int_0^1 dy \frac{1}{y} \int_{\mathrm{Max}\left(\frac{z-(1-y)}{y}, -1\right)}^{\mathrm{Min}\left(\frac{z+(1-y)}{y}, 1\right)} dz \; \theta\left\{ \frac{\zeta - m^2 + \frac{1-z^2}{4} t}{y} + M(z')^2 - [M(z') + \mu]^2 \right\}$$

$$\times \bar{\rho}\left[\frac{\zeta - m^2 + \frac{1-z^2}{4}t}{y} + m^2 - \frac{1-z'^2}{4}t, z'\right] \qquad (A.18)$$

We need the following properties of this spectral function:

$$\rho(\zeta, z) \underset{\zeta\to\infty}{\sim} \zeta^{-\alpha(t)-1}\rho_\infty(z)$$

$$\rho_\infty(z) \xrightarrow[g^2\to 0]{} ig \qquad (A.19)$$

REFERENCES

[1] G. Tictopoulos and S. B. Treiman, Phys. Rev. D2, 805 (1970) and Phys. Rev. D3, 1037 (1970).

[2] B. Hasslacher, D. K. Sinclair, G. M. Cicuta and R. L. Sugar, Phys. Rev. Letters 25, 1591 (1970).

[3] G. M. Cicuta and R. L. Sugar, Phys. Rev. D3, 970 (1971).

[4] B. Hasslacher and D. K. Sinclair, Phys. Rev. D3, 1170 (1971).

[5] S.-J. Chang and T.-M. Yan, Phys. Rev. D4, 537 (1971).

[6] H. Cheng and T. T. Wu, Phys. Rev. D5, 3170 (1972) and Phys. Rev. D6, 1693 (1972).

[7] A. R. Swift, Phys. Rev. D5, 1400 (1972).

[8] S.-J. Chang and P. M. Fishbane, Phys. Rev. D2, 1104 (1970).

[9] H. Cheng and T. T. Wu, Phys. Rev. 186, 1611 (1970), and Phys. Rev. D1, 2775 (1970).

[10] S. Mandelstam, Nuovo Cim. 30, 1127 and 1148 (1963).

[11] H. Rothe, Phys. Rev. 159, 1471 (1967).

[12] V. N. Gribov, Journ. Theor. Exp. Phys. 53, 654 (1967) (Russian).

[13] G. Kramer and K. Meetz, Comm. Math. Phys. 3, 29 (1966).

[14] N. Nakanishi, Phys. Rev. 159, 1471 (1967).

[15] J. C. Polkinghorne, Journ. Math. Phys., 4, 503 (1963); T. L. Trueman, and T. Yao, Phys. Rev. 132, 274 (1963); P. G. Federbush and M. T. Grisaru, Ann. Phys. 22, 263 (1963); B. W. Lee and R. F. Sawyer, Phys. Rev. 127, 2266 (1962).

[16] R. J. Eden, P. V. Polkinghorne, D. I. Olive and J. C. Polkinghorne, Cambridge Press 1966, "The Analytic S-Matrix".

[17] R. E. Cutcosky, Journ. Math. Phys. 1, 429 (1960).

[18] V. N. Gribov and A. A. Migdal, Jadern. Phys. 8, 1002 (1968) (Russian).

[19] P. V. Lanshoff, DAMTP 69/30.

FIGURE CAPTIONS

Fig. 1 S-channel iteration of reggeon exchange: the reggeon legs are crossed in all possible ways.

Fig. 2 (a) The Mandelstam graph; (b) Amati-Fubini-Stangellini (AFS) diagram.

Fig. 3 The four structures of reggeon-particle coupling (upper part) that contributes to the two-reggeon exchange.

Fig. 4 A non-nested structure.

Fig. 5 Reggeon-particle → Reggeon-particle amplitude.

Fig. 6 Two particle -- n-reggeon amplitude.

Fig. 7 Momentum notation for a two-particle n-reggeon coupling.

Fig. 8 A maximal-nested reggeon-particle coupling.

Fig. 9 Decomposition of the reggeon-particle → reggeon-particle amplitude into intermediate states.

Fig. 10 Bethe-Salpeter equation for the sum of ladder graphs.

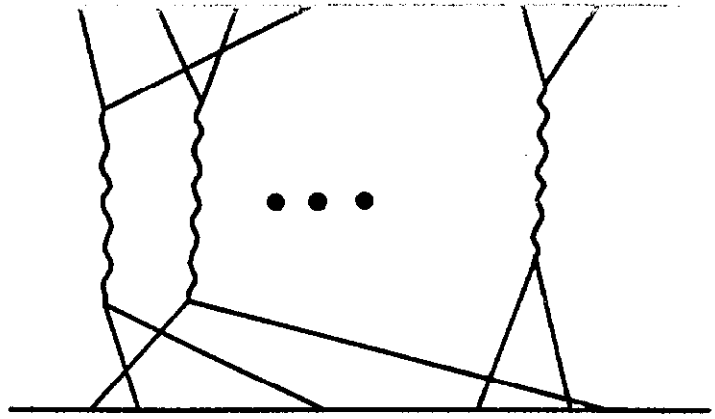

FIG. 1

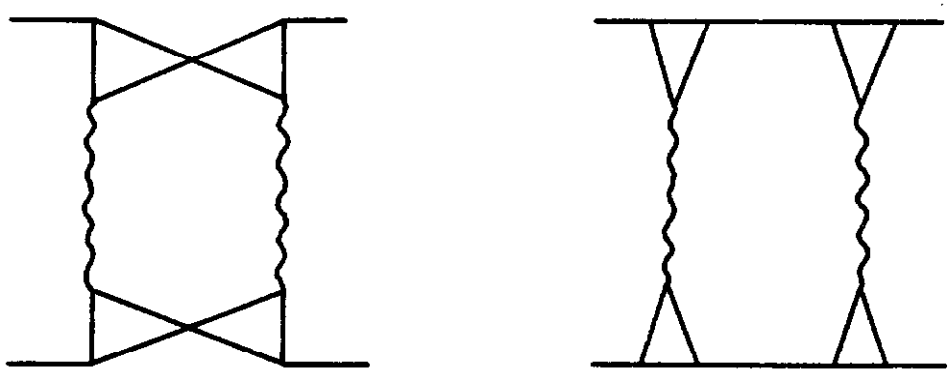

FIG. 2

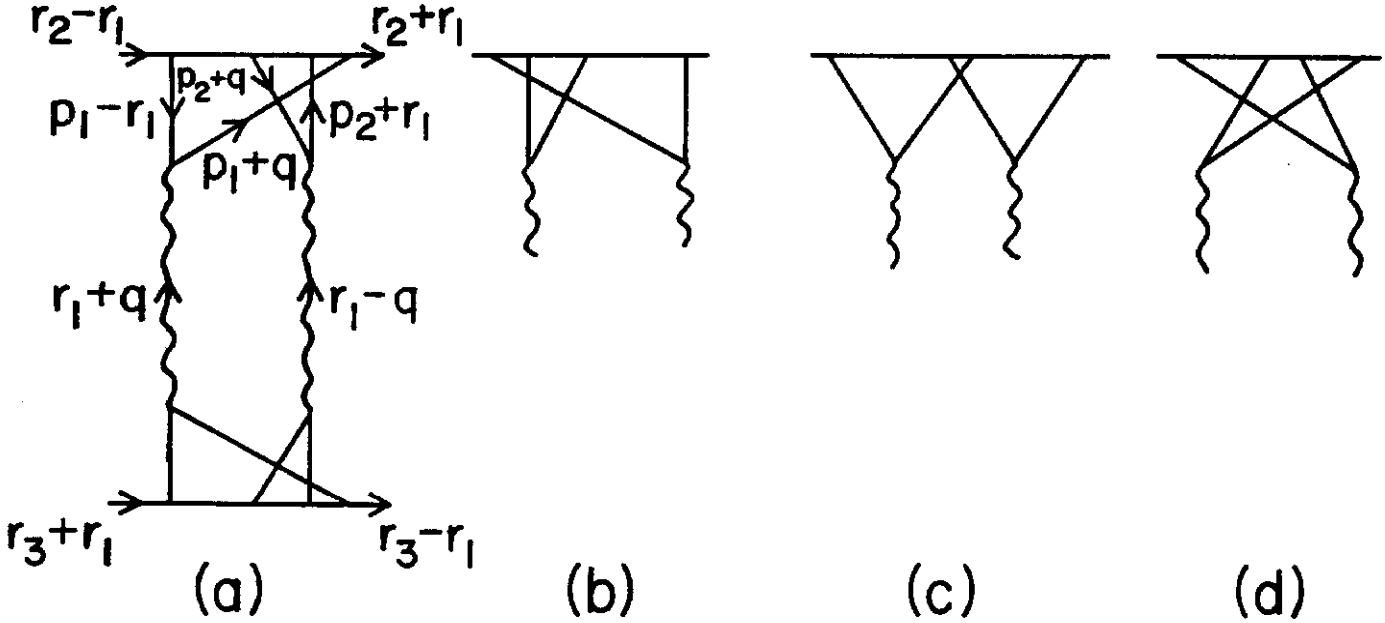

FIG. 3

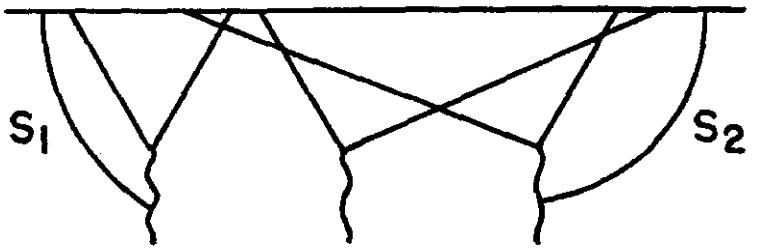

FIG. 4

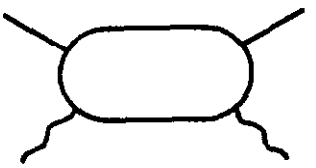

FIG. 5

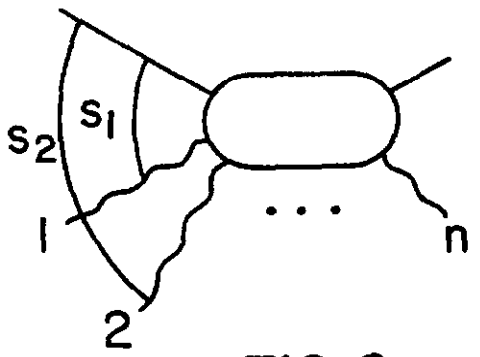

FIG. 6

$(q_{ij} = q_{ji}\ ,\ -q_{10} = q_{nn+1} = r_1)$

FIG. 7

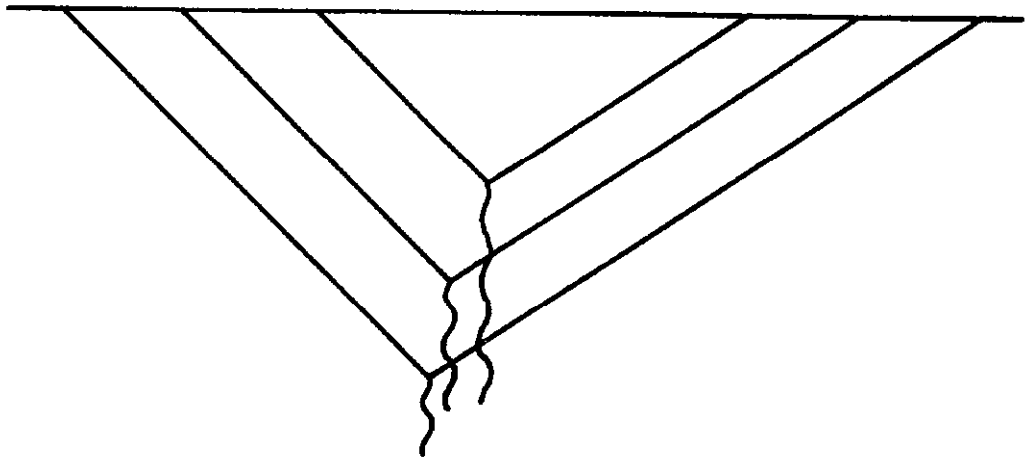

FIG. 8

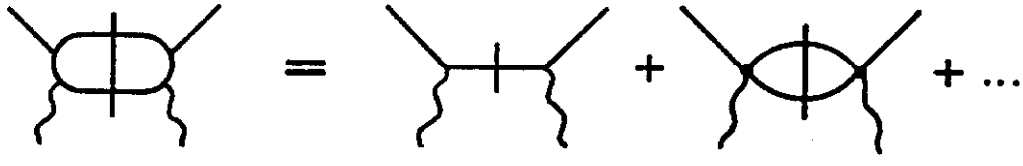

FIG. 9

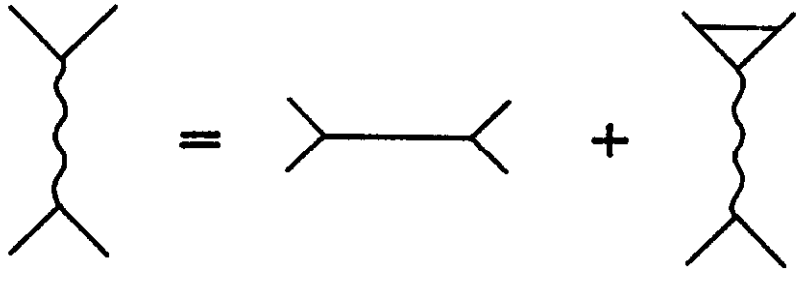

FIG. 10